# Metal Binding Domains 3 and 4 of the Wilson Disease Protein: Solution Structure and Interaction with the Copper(I) Chaperone HAH1[†,‡]

Lucia Banci,[§] Ivano Bertini,[*,§] Francesca Cantini,[§] Amy C. Rosenzweig,[||] and Liliya A. Yatsunyk[||]

*Magnetic Resonance Center (CERM), University of Florence, Via L. Sacconi 6, 50019 Sesto Fiorentino, Italy, Department of Chemistry, University of Florence, Via della Lastruccia 3, 50019 Sesto Fiorentino, Italy, and Department of Biochemistry, Molecular Biology, and Cell Biology and Department of Chemistry, Northwestern University, Evanston, Illinois 60208*

*Received March 19, 2008; Revised Manuscript Received May 22, 2008*

ABSTRACT: The Wilson disease protein or ATP7B is a $P_{1B}$-type ATPase involved in human copper homeostasis. The extended N-terminus of ATP7B protrudes into the cytosol and contains six Cu(I) binding domains. This report presents the NMR structure of the polypeptide consisting of soluble Cu(I) binding domains 3 and 4. The two domains exhibit ferredoxin-like folds, are linked by a flexible loop, and act independently of one another. Domains 3 and 4 tend to aggregate in a concentration-dependent manner involving nonspecific intermolecular interactions. Both domains can be loaded with Cu(I) when provided as an acetonitrile complex or by the chaperone HAH1. HAH1 forms a 70% complex with domain 4 that is in fast exchange with the free protein in solution. The ability of HAH1 to form a complex only with some domains of ATP7B is an interesting property of this class of proteins and may have a signaling role in the function of the ATPases.

Human ATP7B (WLN)[1] is a member of the $P_{1B}$-type ATPase family that plays a crucial role in copper transport and homeostasis in the body (*1*). The WLN protein, like the other human copper ATPase, the Menkes protein (MNK hereafter), delivers copper to the secretory pathway of the trans-Golgi network (TGN) where the metal ion is incorporated into copper-dependent enzymes (*2, 3*). Both proteins can also translocate from the Golgi membrane to the plasma membrane for copper efflux from the cell (*4–6*). The predicted topological organization of WLN and MNK includes four major regions or domains: the N-terminal copper binding domain, the transmembrane domain, the ATP binding domain, and the actuator domain.

The ~650-amino acid N-terminal domain of WLN (WLN16, hereafter) contains six soluble domains with a conserved metal binding motif GMT/HCxxCxxxIE, each capable of binding 1 equiv of Cu(I) with similar affinity (*7–12*). The N-termini of WLN homologues from other organisms contain between one and five metal binding domains (*13*). Although the structure of WLN16 has yet to be determined, the NMR structure of a construct containing domains 5 and 6 (WLN56) is available (*14*). The two domains each have a ferredoxin-like fold ($\beta\alpha\beta\beta\alpha\beta$), are connected by a short linker, and are found in a fixed reciprocal orientation.

The six soluble domains of both WLN and MNK receive copper from the cytoplasmic metallochaperone HAH1 (*15*). The exact role and interplay of the six soluble domains are still unclear. In the case of MNK, the six soluble domains interact differently with HAH1. The interactions have been investigated by a variety of techniques, ranging from yeast two-hybrid assays (*16–18*) to NMR (*19, 20*). These data indicate that the MNK first and fourth domains form a metal-mediated adduct with HAH1 whereas the sixth domain is simultaneously loaded with Cu(I) without formation of the adduct. In the case of WLN, both the second and fourth domains can form a copper-dependent adduct with HAH1 (*14, 16, 18, 21*). By contrast, WLN56 can receive Cu(I) from domain 4, but not from HAH1 (*14*). In another report, a series of six-domain constructs in which five of the six metal binding CXXC motifs were mutated to SXXS was generated (*11*). In all constructs, the intact domain was able to receive Cu(I) from HAH1. We report here the structural and dynamical characterization of a construct containing WLN domains 3 and 4 (WLN34 hereafter) as well as their interaction with Cu(I) and Cu(I) HAH1.

## MATERIALS AND METHODS

*Preparation of Protein Samples.* A DNA segment corresponding to residues 238−439 of WLN was amplified by PCR, cloned into the pET32Xa/LIC vector, and transformed into Rosetta(DE3)pLysS cells. The resulting construct is 202

[†] This work was supported by National Institutes of Health Grant GM58518, Integrated Project SPINE2-COMPLEXES n° 031220, UPMAN n° LSHG-CT-2004-512052, and Ente Cassa di Risparmio di Firenze.

[‡] Resonance assignments and the atomic coordinates for the NMR structures of apo-WLN34 have been deposited in BioMagResBank (entry 11041) and Protein Data Bank, respectively (entry 2ROP).

* To whom correspondence should be addressed: Magnetic Resonance Center, University of Florence, Via L. Sacconi, 6 50019 Sesto Fiorentino, Italy. Fax: +39 055 4574271. Telephone: +39 055 4574272. E-mail: ivanobertini@cerm.unifi.it.

[§] University of Florence.

[||] Northwestern University.

[1] Abbreviations: rmsd, root-mean-square deviation; NOE, nuclear Overhauser effect; HSQC, heteronuclear single-quantum coherence; WLN, human Wilson disease protein or ATP7B; MNK, human Menkes disease protein or ATP7A; WLN16, N-terminal metal binding domain of WLN; WLN56, two-domain construct comprising the fifth and sixth metal binding domains of WLN; WLN34, two-domain construct comprising the third and fourth metal binding domains of WLN; TGN, trans-Golgi network.

10.1021/bi8004736 CCC: $40.75 
Published on Web 06/18/2008

amino acids long and contains domains 3 and 4, the interdomain linker (31 amino acids), a 17-amino acid portion of the linker connecting domains 2 and 3, a 12-amino acid portion of the linker connecting domains 4 and 5, and no tags. For the sake of simplicity, in the following text, residues will be numbered from 1 to 202, rather than starting from 238. Cells were grown at 37 °C in M9 minimal medium containing $(NH_4)_2SO_4$ as the sole nitrogen source and glucose as the sole carbon source. The medium was supplemented with a vitamin mix (Sigma), 100 $\mu$g/mL carbenicillin, and 40 $\mu$g/mL chloramphenicol. The $^{15}$N- and $^{13}$C-enriched samples were produced using >95% enriched nitrogen and carbon sources, as appropriate. When the $OD_{600}$ reached 0.7−0.9, the flasks were cooled to 18 °C, and protein expression was induced with 1 mM isopropyl $\beta$-D-thiogalactopyranoside (IPTG). Cells were harvested after an overnight growth by centrifugation for 15 min at 8000*g*, resuspended in 50 mM HEPES (pH 8.0), 150 mM NaCl, 0.1% Triton X-100, and 1 mM phenylmethanesulfonyl chloride (PMSF), and stored at −80 °C.

For purification, the cell suspension was thawed and stirred at ambient temperature for 30−60 min with EDTA-free protease inhibitor tablets (Roche, one tablet for 40 mL of cell suspension), 1 mM PMSF, and a pinch of solid DNaseI. The solution was centrifuged at 125000*g* for 30−60 min, and the supernatant was applied to a 20 mL nickel-loaded Chelating Sepharose column (Pharmacia) rinsed with buffer A [50 mM HEPES (pH 7.5), 500 mM NaCl, and 10% glycerol]. WLN34 was eluted with a 4 column volume gradient from 90 to 300 mM imidazole (pH 7.5) with 500 mM NaCl and dialyzed twice (with at least one overnight dialysis) at 4 °C versus 2 L of buffer H [50 mM HEPES (pH 7.5) and 200 mM NaCl]. The protein solution was then concentrated to 50 mL (~40 $\mu$M), and cleavage of affinity tags was initiated by the addition of 120 units of Factor Xa (Novagen) in buffer H supplemented with 5 mM $CaCl_2$ at room temperature. The cleavage was stopped after 3 h by addition of 1 mM PMSF. The protein was loaded onto the nickel column preequilibrated with buffer A and eluted with ~36 mM imidazole. Fractions containing the cleaved protein were concentrated in the presence of 1 mM EDTA, 10 mM DTT, and 50 $\mu$M bathocuproine disulfonate (BCS), applied to a Superdex 200 gel filtration column (Pharmacia), and eluted with 20 mM sodium phosphate (pH 6.5) and 150−200 mM NaCl. The typical yield was ~5 and ~11 mg of pure protein per liter of *Escherichia coli* culture for $^{13}$C- and $^{15}$N-labeled and $^{15}$N-labeled samples, respectively. The identity of the protein was confirmed by mass spectrometry, and the purity was assessed by SDS−PAGE. The Cu(I) HAH1 sample was prepared as described previously, always without a $His_6$ tag (*22*).

The copper-loaded WLN34 was prepared by adding up to 2 equiv of the Cu(I) acetonitrile complex $[Cu(CH_3CN)_4PF_6)]$ to apoprotein that had been reduced with 2−3 molar equiv of dithiothreitol (DTT). $Cu(CH_3CN)_4PF_6$ was added in a $N_2$ atmosphere chamber and the titration followed via $^1$H−$^{15}$N HSQC NMR spectra. Binding of Cu(I) was confirmed by atomic absorption spectroscopy. Titrations of [$^{15}$N]WLN34 with both unlabeled Cu(I) HAH1 and Cu(I)-[$^{15}$N]HAH1 with a molar ratio of HAH1 to WLN34 of up to 3:1 were performed similarly. In addition, $^{15}$N-labeled Cu(I) WLN34 was titrated with unlabeled apo-HAH1 at an HAH1:WLN34 molar ratio of up to 2:1.

*NMR Experiments and Structure Calculations.* The NMR spectra were recorded at 298 K on Avance 500, 700, and 900 Bruker spectrometers, all equipped with cryogenically cooled probes. Resonance assignments of apo-WLN34 and Cu(I) WLN34 were performed by conventional multidimensional NMR techniques based on triple-resonance experiments (Table S1) (*23*). All residues were assigned, with the exception of Ser17, His30, Lys32, Arg76, and Thr132 for apo-WLN34 and Met29, His30, Lys32−Cys34, and Arg76 for Cu(I) WLN34. Resonance assignments are reported as Supporting Information (Tables S2 and S3) and have been deposited in the BioMagResBank (entry 11041). Distance constraints for structure determination of apo-WLN34 were obtained from $^{15}$N-edited and $^{13}$C-edited three-dimensional NOESY-HSQC experiments (Table S1). Structure calculations were performed using CYANA (*24*). Each of the 20 conformers with the lowest residual CYANA target function value was then energy-minimized in explicit solvent with AMBER-8 (*25*). NOE and torsion angle constraints were applied with force constants of 32 kcal $mol^{-1}$ $Å^{-2}$ and 32 kcal $mol^{-1}$ $rad^{-2}$, respectively.

*Heteronuclear Relaxation Data.* The dynamic properties of apo-WLN34 and Cu(I) WLN34 have been directly sampled through $^{15}$N relaxation measurements. $^{15}$N longitudinal and transverse relaxation rates (*26*) and $^{15}$N($^1$H) NOEs (*27*) were recorded at 298 K at 500 MHz, using a protein concentration of 0.1 mM for both apo-WLN34 and Cu(I) WLN34. Relaxation measurements for apo-WLN34 were performed also at a protein concentration of 1 mM. $R_1$ and $R_2$ relaxation rates were obtained by fitting the cross-peak volumes (*I*), measured as a function of the relaxation delay, to a single-exponential decay as described in the literature (*28*). Heteronuclear NOE values were calculated as the ratio of peak volumes in spectra recorded with and without saturation. In all experiments, the water signal was suppressed with the "water flipback" scheme (*27*).

The average backbone $^{15}$N longitudinal $R_1$ and transverse $R_2$ relaxation rates and $^{15}$N{$^1$H} NOE value at 0.1 mM are 1.8 ± 0.1 $s^{-1}$, 11.7 ± 1.5 $s^{-1}$, and 0.71 ± 0.04, respectively, for domain 3 and 1.9 ± 0.2 $s^{-1}$, 10.7 ± 1.8 $s^{-1}$, and 0.72 ± 0.04 for domain 4, respectively (Figure 1). For Cu(I) WLN34, the average relaxation rates and $^{15}$N{$^1$H} NOE value at 0.1 mM are 1.9 ± 0.1 $s^{-1}$, 12.0 ± 2.0 $s^{-1}$, and 0.73 ± 0.04, respectively, for domain 3 and 2.3 ± 0.2 $s^{-1}$, 8.5 ± 1.4 $s^{-1}$, and 0.73 ± 0.05 for domain 4, respectively (Figure 1).

## RESULTS AND DISCUSSION

*Protein Structural and Dynamical Characterization.* A construct containing soluble metal binding domains 3 and 4 of the human WLN protein (WLN34) has been overexpressed, and its structural and Cu(I) binding properties as well as its interaction with HAH1 have been studied by NMR. The NMR spectra of apo-WLN34 and copper-loaded WLN34 are indicative of a folded protein. The two domains consist of ~70 amino acids each and are connected by a linker of 31 residues. The $^1$H−$^{15}$N HSQC spectra show well-dispersed amide signals with few peaks clustered in the random-coil region. Peak assignment indicates that the

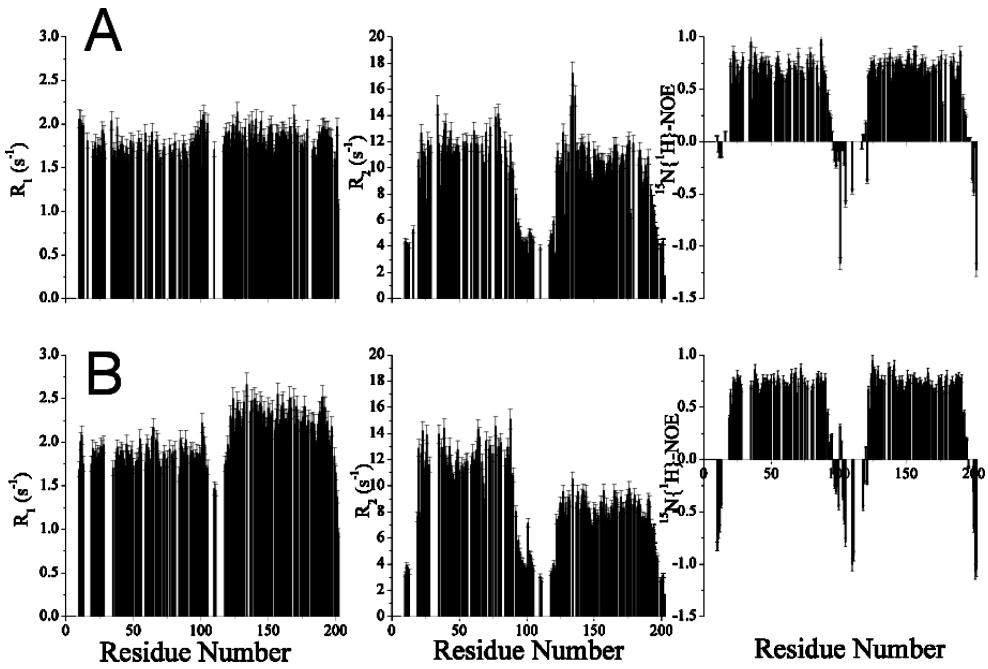


FIGURE 1: $^{15}N$ $R_1$ and $R_2$ relaxation data and $^{15}N\{^1H\}$ NOEs of apo-WLN34 (A) and Cu(I) WLN34 (B) measured at 500 MHz and 298 K on a 0.1 mM sample. The relaxation rates were obtained from the fitting of the cross-peak volumes as a function of the relaxation delays to a single-exponential decay. Heteronuclear NOE values were calculated as the ratio of peak volumes in spectra recorded with and without saturation.

dispersed signals belong to residues of the two domains, confirming their folded state (Figure S1). By contrast, the NH resonances belonging to residues of the linker and to 17 and 12 amino acids located at the N- and C-termini of the construct have reduced signal spreading, which suggests a random-coil-like conformation for these regions (Figure S1). $^{15}N$ relaxation data are consistent with these conformational properties. The residues belonging to the linker region and to the C- and N-terminal regions of both apo and Cu(I)-loaded forms of WLN34 are characterized by significantly negative $^{15}N\{^1H\}$ NOE values, indicating that they experience extensive dynamics on the subnanosecond time scale typical of random-coil regions.

The mobility properties of WLN34 were investigated by performing $^{15}N$ relaxation measurements at different concentrations. A decrease in the correlation time for protein tumbling ($\tau_m$), as estimated from the $R_2/R_1$ ratios, was observed for both domains of apo-WLN34 when the protein concentration was reduced from 1.0 to 0.1 mM. For apo-WLN34, the $\tau_m$ values of domains 3 and 4 were 11.7 $\pm$ 0.9 and 10.6 $\pm$ 0.8 ns, respectively, at 1 mM protein concentration and decreased to 9.0 $\pm$ 0.6 and 8.0 $\pm$ 0.9 ns, respectively, at 0.1 mM protein. These data suggest that some kind of aggregation due to domain−domain interactions, involving both domains 3 and 4, is operative in the apo-WLN34 construct, as the $\tau_m$ value is higher than that expected for a single domain freely reorienting in solution. Since the $\tau_m$ values of both domains decrease with protein concentration, the aggregation phenomena are characterized by intermolecular interactions rather than intraprotein domain−domain interactions. Moreover, the lack of detectable change in the $^1H$ and $^{15}N$ chemical shifts for any residue with a change in concentration indicates that these protein−protein interactions are likely not localized to any specific region of the protein but involve different surface patches. Taken together, the data indicate that aggregation of apo-WLN34 is concentration-dependent and involves nonspecific intermolecular interactions. The behavior of Cu(I) WLN34 is more complex. The $R_1$ and $R_2$ values of domain 3 are similar to those of the apoprotein at the same concentration (0.1 mM protein), and their ratio provides a similar $\tau_m$ value of 8.9 $\pm$ 0.9 ns. However, domain 4 is characterized by a higher $R_1$ value and a lower $R_2$ value, indicative of faster reorientation. Thus, a lower reorientational correlation time of 6.2 $\pm$ 0.9 ns is estimated from their ratio.

Both apo-WLN34 and Cu(I) WLN34 exhibit aggregation before and after 10-fold dilution since the typical $\tau_m$ value of a single soluble copper binding domain is 4.5−5 ns (*22*). Consistent with this observation, the protein precipitated significantly over 2−3 days at concentrations higher than 1 mM. In the presence of Cu(I), domain 4 seems to be less involved in nonspecific interactions with respect to domain 3 and therefore tumbles in solution more freely than in the apo state. The tumbling rate value of domain 4 in Cu(I) WLN34 is similar to that found for a single soluble copper binding domain, indicating that the linker allows free reorientation of the two domains in solution. Overall, the tumbling behavior suggests that domains 3 and 4 of apo-WLN34 are involved in intermolecular interactions with the same domain of another protein molecule and that copper binding disrupts the interdomain interactions of domain 4 but not of domain 3.

The solution structure of apo-WLN34 was determined using 2452 meaningful upper distance limits, 231 angle constraints experimentally determined, and 28 proton pairs stereospecifically assigned. After energy minimization in explicit solvent, the final bundle of 20 conformers of apo-WLN34 has an average (over all conformers) target function of 1.80 $\pm$ 0.08 Å$^2$ (CYANA units). The average backbone rmsd values, over residues 20−90 for domain 3 and 120−190 for domain 4, are 0.58 $\pm$ 0.08 and 0.50 $\pm$ 0.06 Å, respectively (Figure S2). Table S4 reports statistics on

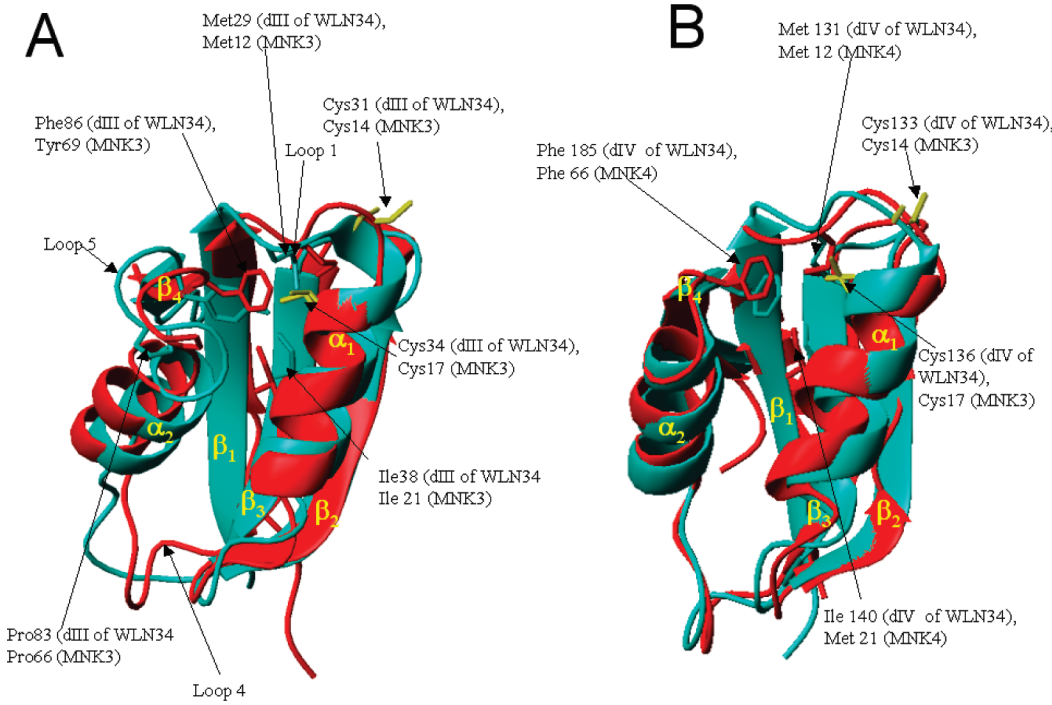


FIGURE 2: Overlays of domains 3 (A) and 4 (B) of apo-WLN34 (red) with the corresponding domains (cyan) of apo-MNK. The side chains of metal binding Cys residues are colored yellow. Some key residues are also shown. Secondary structure elements are labeled. The domain number is given in parentheses (Roman numerals, i.e., dIII and dIV).

restraint violations in the final structure together with structural quality parameters from PROCHECK-NMR (*29*) and WHATIF (*30*). The two domains of apo-WLN34 are well-folded with the ferredoxin-like fold common to all other copper ATPase soluble domains characterized up to now (*14, 31–34*). By contrast, the linker lacks long-range NOEs, consistent with its high flexibility (vide supra) (Figure S3).

Domains 3 and 4 of apo-WLN34 can be superimposed with the single domains 3 and 4 of MNK [MNK3 and MNK4, respectively, hereafter (PDB entries 2G90 and 1AWO, respectively)] (*32, 34*) with global rmsd values of 1.3 and 0.7 Å, respectively, calculated for backbone atoms (Figure 2). The largest structural changes between the forms of domain 3 occur in loop 4, located after the third $\beta$-strand, and in helix $\alpha_1$, which follows the metal binding loop (loop 1) and is shorter in domain 3 of apo-WLN34 than in apo-MNK3 (Figure 2A). Similar to what has been previously observed in the structure of MNK3 (*32*), helix $\alpha_2$ in domain 3 of WLN is shorter at its C-terminus with respect to the other soluble domains of WLN and MNK, structurally distinguishing this domain from the others. This difference is due to a proline residue (Pro83, numbering of the protein studied here) conserved in all forms of domain 3 of mammalian Cu(I)-ATPases. In domains of other Cu(I)-ATPases, this Pro is substituted with a Phe residue which is part of a network of hydrophobic contacts involving the conserved Met located two residues before the metal binding loop, the second metal binding Cys, and a conserved Ile in helix $\alpha_1$ (*31, 35*). This core is present in domain 3 of apo-WLN34 and in MNK3 (*32*), but Phe86 is located four positions closer to the C-terminus than in the other domains. The loop between helix $\alpha_2$ (loop 5) and strand $\beta_4$ is therefore particularly long in domain 3 of both WLN and MNK. Domain 4 of apo-WLN34 (Figure 2B) is very similar to MNK domain 4 (*34*), consistent with their high degree of sequence identity (55%). The metal binding site is stabilized by hydrophobic interactions involving the conserved Phe residue (Phe185, numbering of the protein studied here) located in loop 5. In the metal binding motifs of both domains, the side chains of the two Cys point toward the solvent in a conformation ready to bind the Cu(I) ion.

*Interaction of WLN34 with Cu(I) and with Cu(I) HAH1.* WLN34 binds two Cu(I) ions with similar affinity via the Cys residues of the two metal binding motifs. At substoichiometric Cu(I) concentrations, the amide signals from the metalated form of each domain (3 and 4) in the $^{1}H-^{15}N$ HSQC spectrum have similar intensities (Figure S4). This observation is consistent with the similar binding constants measured for the two domains, WLN3 [$(6.3 \pm 3.2) \times 10^{10}$] and WLN4 [$(2.5 \pm 1.3) \times 10^{10}$], within a six-domain construct (*11*). Variations in the chemical shifts between apo-WLN34 and Cu(I) WLN34 are observed only for the metal binding residues and those in proximity to the metal binding site. These spectral changes indicate that metal binding does not affect the overall fold, producing only minor localized structural changes in the binding loop. A similar effect is observed for all the soluble domains of MNK and WLN (*14, 33–36*). During copper addition, the spectra exhibit two sets of signals arising from the apo and Cu(I)-bound forms of WLN34, indicating that exchange between the two forms is slow on the NMR time scale (equilibration time of less than milliseconds).

To study the interaction between Cu(I) HAH1 and the domains of WLN34, apo-[$^{15}$N]WLN34 was titrated with unlabeled Cu(I) HAH1. This system exhibited a complex and domain-dependent behavior. Both domains 3 and 4 are affected by the addition of even substoichiometric amounts of Cu(I) HAH1 [i.e., with <1 equiv of Cu(I) available for three binding sites, one on HAH1 and two on WLN34] (Figure 3), indicating that the domains have similar affinities

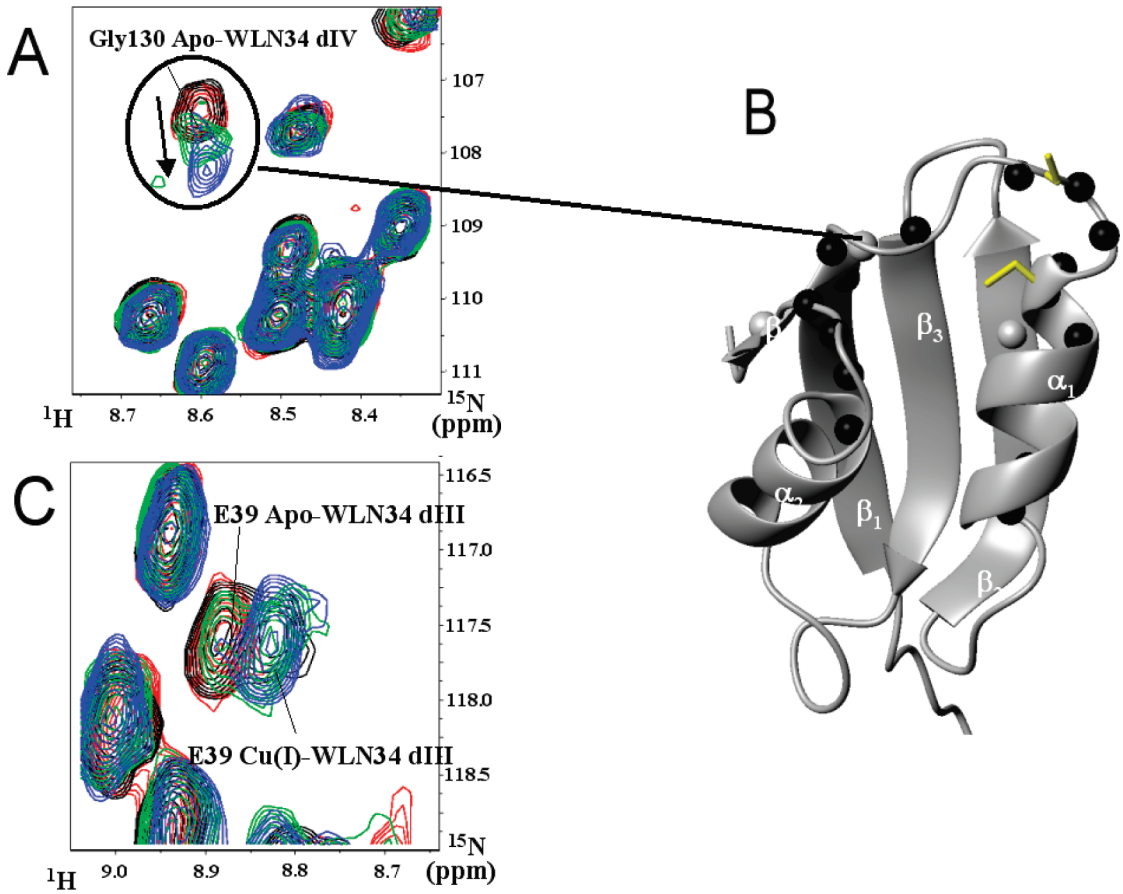


FIGURE 3: (A) Overlay of a selected region of the $^{1}$H−$^{15}$N HSQC spectra of apo-WLN34 (red) and apo-WLN34 in the presence of 0.25 (black), 1 (green), and 2 equiv (blue) of unlabeled Cu(I) HAH1, showing a peak of domain 4 experiencing a variation of the chemical shift along the titration. For the latter peak, a single set of signals was observed throughout the titration. (B) Chemical shift perturbation data mapped onto the solution structure of domain 4 of WLN34. Residues featuring a $\delta\Delta$ value of at least 0.05 ppm are represented as light gray spheres (residues 130, 155, and 188). Black spheres indicate peaks that became broad beyond detection upon interaction (residues 128, 129, 131, 133, 136−138, 140, 143, 145, and 183−186). The side chains of metal binding cysteines are shown, and secondary structure elements are labeled. (C) Overlay of a selected region of the $^{1}$H−$^{15}$N HSQC spectra of apo-WLN34 (red) and apo-WLN34 in the presence of 0.25 (black), 1 (green) and 2 equiv (blue) of unlabeled Cu(I) HAH1, highlighting the presence of both apo and copper(I)-loaded forms of domain 3. For the latter domain, two sets of signals were observed throughout the titration.

for incorporation of Cu(I) from HAH1. However, the effect is different for the two domains. For domain 4, addition of increasing amounts of Cu(I) HAH1 caused changes in the chemical shifts of some backbone NH signals and the disappearance of others (Figure 3A,B). In the case of domain 3, a second set of signals appeared, corresponding to the Cu(I)-bound species, and its intensity increased upon addition of Cu(I) HAH1 (Figure 3C). These data suggest that Cu(I) HAH1 forms detectable amounts of a macromolecular complex with domain 4, whereas domain 3 removes Cu(I) from the metallochaperone without detectable complex formation. Similarly, adduct formation was observed when apo-[$^{15}$N]WLN34 was titrated with increasing amounts of Cu(I)-[$^{15}$N]HAH1. The interaction between $^{15}$N-labeled Cu(I) HAH1 and WLN34 also perturbs the chemical shift of some NH signals of Cu(I) HAH1, confirming complex formation (Figure 4A). A substantial number of signals from residues in HAH1 also became broad beyond detection, indicating that HAH1 interacts with WLN34 at a rate compatible with the NMR time scale.

Cu(I) HAH1 in the mixture has a $\tau_m$ value, as estimated from the $R_2/R_1$ ratios, of 9.6 ± 0.7 ns. This value is consistent with ~70% of the HAH1 molecules participating in a protein−protein adduct, assuming an overall rotational correlation time for molecular tumbling of the complex of 11.1 ns (6.2 ns for the WLN4 domain plus 4.9 ns for HAH1). apo-[$^{15}$N]WLN34 in the presence of 2 equiv of unlabeled Cu(I) HAH1 gives molecular tumbling times of 8.5 ± 0.6 and 9.3 ± 0.6 ns for domains 3 and 4, respectively. These values closely resemble those of apo-WLN34 in the absence of HAH1 (9.0 ± 0.6 ns for domain 3 and 8.0 ± 0.9 ns for domain 4) but differ from that of copper-loaded domain 4 (6.2 ± 0.9 ns). Domain 3 becomes metalated without any appreciable formation of a complex with HAH1. Since both the apo and Cu(I) forms are always involved in nonspecific interactions with another domain 3, as shown by its higher than a single domain $\tau_m$ value, its $\tau_m$ is not expected to change in the presence of HAH1, which is observed experimentally. By contrast, domain 4 with Cu(I) bound is tumbling as an isolated moiety. The observed increase in $\tau_m$ upon Cu(I) HAH1 interaction is thus consistent with formation of a complex between the two proteins as indicated by the chemical shift variations upon titration.

Finally, mapping of the signal perturbations experienced by domain 4 and by HAH1 onto the corresponding solution structures defines regions of intermolecular contact (Figures 3B and 4B). These patches are similar to those determined

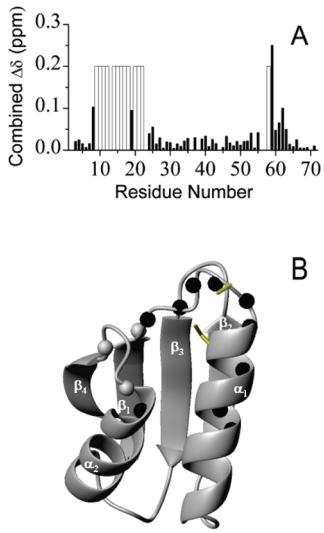


FIGURE 4: (A) Combined chemical shift differences between Cu(I)-bound [$^{15}$N]HAH1 and Cu(I)-bound [$^{15}$N]HAH1 in the presence of 0.5 equiv of apo-[$^{15}$N]WLN34. White bars indicate peaks that became broad beyond detection upon interaction. A $\Delta\delta$ value of 0.2 ppm was arbitrarily assigned to those peaks only for graphical representation. (B) Chemical shift perturbation data mapped onto the solution structure of HAH1 [PDB entry 1TL5 (*22*)]. Residues featuring a $\delta\Delta$ value of at least 0.1 ppm are represented as light gray spheres (residues 8, 59, and 62). Black spheres indicate peaks that became broad beyond detection upon interaction (residues 9−23 and 58). The side chains of metal-binding cysteines are shown, and secondary structure elements are labeled.

for all the other MNK or WLN domains as well as the soluble domains of ATPases from other organisms (*14, 20, 37, 38*).

*Functional Implications.* As part of our efforts to understand the roles of the N-terminal metal binding domains in copper transport by WLN, we determined the NMR structure of WLN34. WLN34 comprises two distinct domains with ferredoxin-like folds. The two domains are connected by a flexible loop and act independently of one another, like "beads on a string", even if some weak, nonspecific interactions with the corresponding domain of another molecule occur. By contrast, electrostatic interactions and hydrogen bonds hold the two domains in WLN56 in a defined and rigid orientation, precluding the possibility of interdomain copper transfer (*14*). Cu(I) HAH1 delivers the metal ion efficiently to WLN34, but not to WLN56 according to NMR (*14*) or the yeast two-hybrid assay (*16*). Furthermore, the interaction with Cu(I) HAH1 is remarkably different for the two domains of WLN34. It is not clear why Cu(I) HAH1 can form stable adducts with domain 4 and not with domain 3, given that Cu(I) is transferred efficiently to both domains. Similar behavior is observed for the six-domain construct of MNK, in which domains 3 and 4 were metalated by Cu(I) HAH1, but only domain 4 formed a stable adduct with Cu(I) HAH1 (*20*). A few possible scenarios are consistent with data. Domain 3 could be metalated by Cu(I) HAH1, possibly through weak interactions. The adduct concentration may be too low for detection by NMR. Alternatively, domain 3 could receive copper from metalated domain 4 [that was loaded via interaction with Cu(I) HAH1]. The two domains are connected by a long flexible linker, rendering interdomain Cu(I) transfer possible. However, site-directed mutagenesis studies on both the MNK16 and WLN16 constructs showed that all the domains can be directly metalated by Cu(I) HAH1 despite differences in the properties for their interaction with the chaperone (*11, 20*).

While the differences in behavior between domains 3 and 4 and between WLN34 and WLN56 could be the basis for the distinct roles of the metal binding domains, the available literature suggests that the functional roles of each of the six metal binding domains in WLN are defined not by the fold or the metal binding properties of each individual domain but by the properties and position of each domain within the global conformation of the entire soluble portion of the ATPase and/or, most probably, by the interaction of the metal binding domains with other components of the ATPase or with the metallochaperone. Therefore, NMR studies of the entire soluble portion of Wilson ATPase and its interactions with Cu(I) and HAH1 are necessary. The current NMR structure of WLN34 combined with the structure of WLN56 lays the foundation for such studies.

## SUPPORTING INFORMATION AVAILABLE

Four figures showing the $^{15}$N−$^{1}$H HSQC spectrum, the number of meaningful NOEs, the overlay of 20 conformers of the apo-WLN34 structure, and the overlay of selected regions of the $^{1}$H−$^{15}$N HSQC spectra of apo-WLN34 and apo-WLN34 in the presence of substoichiometric concentration of copper(I) and four tables showing the experiments performed, the chemical shift assignments, and the statistics on restraint violations in the final structure of apo-WLN34. This material is available free of charge via the Internet at http://pubs.acs.org.

## REFERENCES

1. Bull, P. C., Thomas, G. R., Rommens, J. M., Forbes, J. R., and Cox, D. W. (1993) The Wilson disease gene is a putative copper transporting P-type ATPase similar to the Menkes gene. *Nat. Genet. 5*, 327–337.
2. Harrison, M. D., Jones, C. E., Solioz, M., and Dameron, C. T. (2000) Intracellular copper routing: The role of copper chaperones. *Trends Biochem. Sci. 25*, 29–32.
3. Puig, S., and Thiele, D. J. (2002) Molecular mechanisms of copper uptake and distribution. *Curr. Opin. Chem. Biol. 6*, 171–180.
4. Cater, M. A., La Fontaine, S., Shield, K., Deal, Y., and Mercer, J. F. (2006) ATP7B mediates vesicular sequestration of copper: Insight into biliary copper excretion. *Gastroenterology 130*, 493–506.
5. La Fontaine, S., and Mercer, J. F. (2007) Trafficking of the copper-ATPases, ATP7A and ATP7B: Role in copper homeostasis. *Arch. Biochem. Biophys. 463*, 149–167.
6. Petris, M. J., Voskoboinik, I., Cater, M., Smith, K., Kim, B. E., Llanos, R. M., Strausak, D., Camakaris, J., and Mercer, J. F. (2002) Copper-regulated trafficking of the Menkes disease copper ATPase is associated with formation of a phosphorylated catalytic intermediate. *J. Biol. Chem. 277*, 46736–46742.
7. Lutsenko, S., Petrukhin, K., Cooper, M. J., Gilliam, C. T., and Kaplan, J. H. (1997) N-Terminal domains of human copper-transporting adenosine triphosphatases (the Wilson's and Menkes disease proteins) bind copper selectively in vivo and in vitro with stoichiometry of one copper per metal-binding repeat. *J. Biol. Chem. 272*, 18939–18944.
8. DiDonato, M., Narindrasorasak, S., Forbes, J. R., Cox, D. W., and Sarkar, B. (1997) Expression, purification, and metal binding properties of the N-terminal domain from the Wilson disease putative copper-transporting ATPase (ATP7B). *J. Biol. Chem. 272*, 33279–33282.
9. Bull, P. C., and Cox, D. W. (1994) Wilson disease and Menkes disease: New handles on heavy-metal transport. *Trends Genet. 10*, 246–252.
10. Banci, L., and Rosato, A. (2003) Structural genomics of proteins involved in copper homeostasis. *Acc. Chem. Res. 36*, 215–221.

11. Yatsunyk, L. A., and Rosenzweig, A. C. (2007) Copper(I) binding and transfer by the N-terminus of the Wilson disease protein. *J. Biol. Chem. 282*, 8622–8631.
12. Wernimont, A. K., Yatsunyk, L. A., and Rosenzweig, A. C. (2004) Binding of copper(I) by the Wilson disease protein and its copper chaperone. *J. Biol. Chem. 279*, 12269–12276.
13. Arnesano, F., Banci, L., Bertini, I., Ciofi-Baffoni, S., Molteni, E., Huffman, D. L., and O'Halloran, T. V. (2002) Metallochaperones and metal transporting ATPases: A comparative analysis of sequences and structures. *Genome Res. 12*, 255–271.
14. Achila, D., Banci, L., Bertini, I., Bunce, J., Ciofi-Baffoni, S., and Huffman, D. L. (2006) Structure of human Wilson protein domains 5 and 6 and their interplay with domain 4 and the copper chaperone HAH1 in copper uptake. *Proc. Natl. Acad. Sci. U.S.A. 103*, 5729–5734.
15. Hamza, I., Schafer, M., Klomp, L. W., and Gitlin, J. D. (1999) Interaction of the copper chaperone HAH1 with the Wilson disease protein is essential for copper homeostasis. *Proc. Natl. Acad. Sci. U.S.A. 96*, 13363–13368.
16. Larin, D., Mekios, C., Das, K., Ross, B., Yang, A. S., and Gilliam, C. T. (1999) Characterization of the interaction between the Wilson and Menkes disease proteins and the cytoplasmic copper chaperone, HAH1p. *J. Biol. Chem. 274*, 28497–28504.
17. Strausak, D., Howie, M. K., Firth, S. D., Schlicksupp, A., Pipkorn, R., Multhaup, G., and Mercer, J. F. (2003) Kinetic analysis of the interaction of the copper chaperone Atox1 with the metal binding sites of the Menkes protein. *J. Biol. Chem. 278*, 20821–20827.
18. van Dongen, E. M., Klomp, L. W., and Merkx, M. (2004) Copper-dependent protein-protein interactions studied by yeast two-hybrid analysis. *Biochem. Biophys. Res. Commun. 323*, 789–795.
19. Banci, L., Bertini, I., Cantini, F., Chasapis, C., Hadjiliadis, N., and Rosato, A. (2005) A NMR study of the interaction of a three-domain construct of ATP7A with copper(I) and copper(I)-HAH1: The interplay of domains. *J. Biol. Chem. 280*, 38259–38263.
20. Banci, L., Bertini, I., Cantini, F., Della Malva, N., Migliardi, M., and Rosato, A. (2007) The different intermolecular interactions of the soluble copper-binding domains of the Menkes protein, ATP7A. *J. Biol. Chem. 282*, 23140–23146.
21. Walker, J. M., Huster, D., Ralle, M., Morgan, C. T., Blackburn, N. J., and Lutsenko, S. (2004) The N-terminal metal-binding site 2 of the Wilson's disease protein plays a key role in the transfer of copper from Atox1. *J. Biol. Chem. 279*, 15376–15384.
22. Anastassopoulou, J., Banci, L., Bertini, I., Cantini, F., Katsari, E., and Rosato, A. (2004) Solution structure of the apo- and copper(I) loaded human metallo-chaperone HAH1. *Biochemistry 43*, 13046–13053.
23. Grzesiek, S., and Bax, A. (1993) Amino acid type determination in the sequential assignment procedure of uniformly $^{13}C/^{15}N$-enriched proteins. *J. Biomol. NMR 3*, 185–204.
24. Guntert, P. (2004) Automated NMR structure calculation with CYANA. *Methods Mol. Biol. 278*, 353–378.
25. Case, D. A., Darden, T. A., Cheatham, T. E., Simmerling, C. L., Wang, J., Duke, R. E., Luo, R., Merz, K. M., Wang, B., Pearlman, D. A., Crowley, M., Brozell, S., Tsui, V., Gohlke, H., Mongan, J., Hornak, V., Cui, G., Beroza, P., Schafmeister, C. E., Caldwell, J. W., Ross, W. S., and Kollman, P. A. (2004) AMBER 8, University of California, San Francisco.
26. Farrow, N. A., Muhandiram, R., Singer, A. U., Pascal, S. M., Kay, C. M., Gish, G., Shoelson, S. E., Pawson, T., Forman-Kay, J. D., and Kay, L. E. (1994) Backbone dynamics of a free and phosphopeptide-complexed Src homology 2 domain studied by $^{15}N$ NMR relaxation. *Biochemistry 33*, 5984–6003.
27. Grzesiek, S., and Bax, A. (1993) The importance of not saturating $H_2O$ in protein NMR. Application to sensitivity enhancement and NOE measurements. *J. Am. Chem. Soc. 115*, 12593–12594.
28. Mandel, M. A., Akke, M., and Palmer, A. G., III (1995) Backbone dynamics of *Escherichia coli* ribonuclease HI: Correlations with structure and function in an active enzyme. *J. Mol. Biol. 246*, 144–163.
29. Laskowski, R. A., MacArthur, M. W., Moss, D. S., and Thornton, J. M. (1993) PROCHECK: A program to check the stereochemical quality of protein structures. *J. Appl. Crystallogr. 26*, 283–291.
30. Vriend, G. (1990) WHAT IF: A molecular modeling and drug design program. *J. Mol. Graphics 8*, 52–56.
31. Banci, L., Bertini, I., Cantini, F., Migliardi, M., Rosato, A., and Wang, S. (2005) An atomic level investigation of the disease-causing A629P mutant of the Menkes protein ATP7A. *J. Mol. Biol. 352*, 409–417.
32. Banci, L., Bertini, I., Cantini, F., Della Malva, N., Rosato, A., Herrmann, T., and Wüthrich, K. (2006) Solution structure and intermolecular interactions of the third metal-binding domain of ATP7A, the Menkes disease protein. *J. Biol. Chem. 281*, 29141–29147.
33. Banci, L., Bertini, I., Chasapis, C., Ciofi-Baffoni, S., Hadjiliadis, N., and Rosato, A. (2005) An NMR study of the interaction between the human copper(I) chaperone and the second and fifth metal-binding domains of the Menkes protein. *FEBS J. 272*, 865–871.
34. Gitschier, J., Moffat, B., Reilly, D., Wood, W. I., and Fairbrother, W. J. (1998) Solution structure of the fourth metal-binding domain from the Menkes copper-transporting ATPase. *Nat. Struct. Biol. 5*, 47–54.
35. Banci, L., Bertini, I., Del Conte, R., D'Onofrio, M., and Rosato, A. (2004) Solution structure and backbone dynamics of the Cu(I) and apo-forms of the second metal-binding domain of the Menkes protein ATP7A. *Biochemistry 43*, 3396–3403.
36. DeSilva, T. M., Veglia, G., and Opella, S. J. (2005) Solution structures of the reduced and Cu(I) bound forms of the first metal binding sequence of ATP7A associated with Menkes disease. *Proteins 61*, 1038–1049.
37. Banci, L., Bertini, I., Cantini, F., Felli, I. C., Gonnelli, L., Hadjiliadis, N., Pierattelli, R., Rosato, A., and Voulgaris, P. (2006) The Atx1-Ccc2 complex is a metal-mediated protein-protein interaction. *Nat. Chem. Biol. 2*, 367–368.
38. Arnesano, F., Banci, L., Bertini, I., Cantini, F., Ciofi-Baffoni, S., Huffman, D. L., and O'Halloran, T. V. (2001) Characterization of the binding interface between the copper chaperone Atx1 and the first cytosolic domain of Ccc2 ATPase. *J. Biol. Chem. 276*, 41365–41376.


BI8004736